Interaction Notes

Note 161

October 1973

The Singularity Expansion Method as Applied to Perpendicular Crossed Cylinders in Free Space

Terry T. Crow
Billy D. Graves
Clayborne D. Taylor
Mississippi State University
Mississippi State, Mississippi 39762

ABSTRACT

The singularity expansion method (SEM) has been applied to a system of Pocklington-type integro-differential equations representing perpendicular crossed cylinders. The SEM characteristics of this structure have been studied as the various parameters are varied. The time domain response of one particular geometry has been obtained by SEM and compared to that determined by the more conventional frequency domain analysis and Fourier inversion.

ACKNOWLEDGEMENTS

Discussions with the following persons have proven to be interesting, enlightening, stimulating, as well as helpful: Drs. Carl Baum, Fred Tesche, Don Wilton, Tom Shumpert, and Lennart Marin.

1. Introduction

The singularity expansion method (SEM) as first discussed by Baum [1] has been elaborated and applied in a series of recent notes [2-6]. Using SEM it is possible to determine the time domain scattering from a conducting object in terms of a summation of damped sinusoids. This technique appears to be particularly advantageous in treating scattering from wire configurations that may be useful to model complex physical structures such as aircraft. In this report SEM is applied to determine the current and charge induced on a system of two perpendicular crossed thin cylinders (wires) in free space. This configuration may be viewed as a crude model of an aircraft. The induced current and charge are considered as various parameters of the problem are varied.

In the application of SEM to determine the time domain response of the induced currents it is conventional to derive an integral equation for the induced current and to render it into matrix form by use of the method of moments. Although this procedure is quite straight forward it may consume excessive amounts of time in computation, especially if a parametric study such as the one reported here is performed. Attempting to circumvent this difficulty the writers investigated an alternative to the conventional technique. It was observed that if the current distribution on a current filament is sinusoidal, then exact analytical expressions for the accompaning fields are available. Thus the current induced on a wire configuration can be segmented into sinusoidal current filaments, and the exact analytical expressions can be used to determine the scattered electric and magnetic fields. By requiring the component of the incident plus the

scattered electric field tangent to the wire axis to be zero on the wire axis a system of linear equations is obtained for the wire currents. This procedure was found to be extremely efficient. Moreover, it was also possible to treat solid wires with end caps. The charge distribution on the wires is obtained via the equation of continuity.

Computations for the currents on two perpendicular crossed wires are made, and the data are compared with that obtained using the conventional integral equation solution technique. In general the results agree within a few percent difference. Interesting results with regard to the charge distribution at the wire junction are obtained. These results indicate that the treatment of wire junctions by some investigators may not be correct--at least for certain wire parameters.

The singularity expansions for the wire currents and charges are expressed in terms of the complex natural frequencies, vector current modes, coupling vectors and coupling coefficients. The variation of these quantities with changes in the wire configuration is presented.

2. Formulation

As mentioned in the foregoing the exact field about a currentfilament with a sinusoidal variation of the current along the filament is used. The axial component of the electric field is

$$\hat{r}_{21} \cdot \bar{E}(\bar{r}) = \frac{1}{4\pi\epsilon s} \left[I'(\bar{r}_1) \frac{e^{-s|\bar{r} - \bar{r}_1|/c}}{|\bar{r} - \bar{r}_1|} - I'(\bar{r}_2) \frac{e^{-s|\bar{r} - \bar{r}_2|/c}}{|\bar{r} - \bar{r}_2|} \right] \qquad (1)$$

for the complex Laplacian frequency $s = \sigma + j\omega$ and a filament extending from $\bar{r} = \bar{r}_1$ to $\bar{r} = \bar{r}_2$, where I' is the axial derivative of the current and

$$\hat{r}_{21} = \frac{\bar{r}_2 - \bar{r}_1}{|\bar{r}_2 - \bar{r}_1|}$$

The corresponding radial component of the electric field is

$$\hat{\rho}_{21} \cdot \bar{E}(\bar{r}) = \frac{1}{4\pi\varepsilon s\rho_{21}} \{\hat{r}_{21} \cdot [(\bar{r}-\bar{r}_2)I'(\bar{r}_2) \frac{e^{-s|r-r_2|/c}}{|\bar{r} - \bar{r}_2|}$$

$$- (\bar{r} - \bar{r}_1)I'(\bar{r}_1) \frac{e^{-s|\bar{r} - \bar{r}_1|/c}}{|\bar{r} - \bar{r}_1|}] - \frac{s}{c}[I(\bar{r}_2)e^{-s|\bar{r}-\bar{r}_2|/c}$$

$$- I(\bar{r}_1)e^{-s|\bar{r} - \bar{r}_1|/c}]\} \qquad (2)$$

where ρ_{21} is the radial variable corresponding to the radial variable of a cylindrical coordinate system with the z axis coincident with the axis of the filament. Using (1) and (2) to determine the scattered electric field it is possible to develop a linear system of equations to determine the currents. If the wires are solid then the end cap contributions should be added to both (1) and (2) as discussed in reference [9].

To derive the system of equations for the current distribution on the perpendicular crossed wires the wires are divided into segments. The current on the kth segment of the mth wire is represented

$$I_{mk}(x) = \frac{\alpha_k \sinh[s(x_{k+1} - x)/c] + \alpha_{k+1} \sinh[s(x - x_k)/c]}{\sinh[s(x_{k+1} - x_k)/c]} \qquad (3)$$

Note that α_k is the axial current at $x = x_k$, where x is the variable along any particular wire. Next (3) is used in (1) and (2) to obtain

the components of the scattered electric field about the crossed wires. These components are added to the corresponding incident electric field components to obtain the total electric field. To obtain the system of linear equations for the α_k's, the component of the total electric field tangent to the wire axis is set equal to zero at a discrete set of points along the axes of both wires. For best results these points are selected to be the end points of the aforementioned segments. In addition to the foregoing the junction currents were required to satisfy the Kirchhoff circuit law.

The resulting system of linear equations for the wire currents can be written in the form

$$\overline{\overline{Z}}(s)\ \overline{J}(s) = \overline{E}(s) \tag{4}$$

where $\overline{\overline{Z}}(s)$ is a square system matrix, $\overline{J}(s)$ is a column matrix whose elements are the currents, α_k's , and $\overline{E}(s)$ is a column matrix whose elements are the values of the incident field components evaluated on the wire axes at the end points of the wire segments. According to the singularity expansion method of solution, the current vector may be expressed

$$\overline{J}(s) = \sum_{\alpha} \eta_{\alpha} \frac{1}{s - s_{\alpha}} E_o(s)\overline{\nu}_{\alpha} \tag{5}$$

where $E_o(s)$ is the Laplace transform of the incident pulse, s_{α} are the complex natural frequencies or poles defined as the zeros of the determinant of the system matrix, i. e.

$$\det[\overline{\overline{Z}}(s_{\alpha})] = 0 \ , \tag{6}$$

$\bar{\nu}_\alpha$ are the natural modes that are obtained by solving

$$\bar{\bar{Z}}(s_\alpha)\,\bar{\nu}_\alpha = 0 \quad , \tag{7}$$

and η_α are the coupling coefficients defined

$$\eta_\alpha\, E_o(s)\bar{\nu}_\alpha = \lim_{s\to s_\alpha} (s - s_\alpha)[\bar{\bar{Z}}(s)]^{-1}\,\bar{E}(s) \tag{8}$$

The computational details of the calculation of the foregoing quantities are described in [6]. The charge distribution on the wires is obtained via the equation of continuity,

$$\text{div}\,\bar{J} = -\frac{\partial}{\partial t}\rho \tag{9}$$

Applying the Laplace transform to (9) and using (5) yields

$$\bar{\rho}(s) = \sum_\alpha \eta_\alpha \frac{1}{s - s_\alpha} \frac{E_o(s)}{s} \bar{\nu}_\alpha^{(\rho)} \tag{10}$$

where $\bar{\nu}_\alpha^{(\rho)}$ is a column vector whose elements are the negative spacial derivatives of the currents evaluated at the same points as the current elements of $\bar{\nu}_\alpha$*. In general the $\bar{\nu}_\alpha$ elements were normalized so that the element with the largest absolute value was set equal + 1. These elements were then used to determine $\bar{\nu}_\alpha^{(\rho)}$ according to the foregoing definition.

For a simple step pulse incident on the wire configuration

$$E_o(s) = \frac{E_o}{s} \tag{11}$$

---

*The current expansion exhibits discontinuous derivatives at the ends of the current segments. The derivative at those points is considered to be the arithmetic mean of the finite discontinuity.

and using (11) in both (5) and (10) yields the time domain response of the current and charge

$$\bar{J}(t) = \sum_{\alpha} \eta_{\alpha} \frac{E_o}{s_{\alpha}} e^{s_{\alpha} t} \bar{\nu}_{\alpha} \tag{12}$$

and

$$\bar{\rho}(t) = \sum_{\alpha} \eta_{\alpha} \frac{E_o}{s_{\alpha}^2} e^{s_{\alpha} t} \bar{\nu}_{\alpha}(\rho) - \sum_{\alpha} \eta_{\alpha} \frac{E_o}{s_{\alpha}^2} \bar{\nu}_{\alpha}(\rho) \tag{13}$$

Since the poles occurred in complex conjugate pairs (except for those poles on the negative real axis) both (12) and (13) yield real elements for $\bar{J}(t)$ and $\bar{\rho}(t)$. The poles s_{α} were obtained by searching for the zeros of the system matrix determinant in the third quadrant of the complex s-plane (the conjugate poles occurred in the fourth quadrant). To account for the contribution of the conjugate poles (12) and (13) were evaluated by using only the poles in the third quadrant, taking only the real part of the sum over α and multiplying the final value for the sum by a factor of two.

Before applying the SEM two additional operations are performed. First, instead of excitation by a single incoming plane wave, the excitation by two incoming waves is considered as in [7]. Thus the problem can be broken into a symmetric part and an anti-symmetric part, and by using such conditions the number of current segments that must be carried in the calculations can be reduced. Second the end currents are not assumed zero and uniform end charge distributions are assumed to exist on flat end caps on each wire [8,9].

3. Results

Figure 1 represents the geometry considered and the definition of the parameters in the problem. The reference case is defined as

$$\ell_1'/\ell_1 = 0.5 \ , \ 2\ell_2/(\ell_1 + \ell_1') = 1.0 \ , \ 2\ell_2/a_2 = 20. \ , \ a_1 = a_2 \ , \ 2\ell_2 = L$$

where the incidence is normal to the plane of the waves with the electric field directed along the y axis (this is the same as used in IN85 [7]).

The first five poles and coupling coefficients obtained for the reference case are given in Table 1. In a related study it has been observed that as the number of zones increased from 6 zones per L to 12 zones per L to 18 zones per L, the pole locations change by about 10% in going from 6 to 12 zones per L but only another 2% in going from 12 to 18 zones per L. In the interest of accuracy these studies reported here were run at 18 zones per L. A representation of the crossed cylinder geometry in a three dimensional space and two incoming wave vectors is shown in Figure 2. The illumination of the crossed wires is expressed in terms of symmetric and antisymmetric excitation by two incoming plane waves [7] and the appropriate angles of incidence for these waves are indicated in Figure 2. In any discussion of the crossed cylinder problem having the y, z plane as a symmetry plane there are, in reality, two separate problems to be discussed: 1) the crossed wire problem with E field excitation along the y-wire and 2) the isolated cylinder problem with E field excitation along the y-wire. Since Tesche [3] has discussed thoroughly the latter problem, this discussion will emphasize the former. Thus, Table 1 refers to poles obtained for the reference case when the excitation is along the y-wire, and currents and charges will be induced on each wire in the system. Figure 3 shows the pole behaviors as the

crossing point moves along wire 1 from near one end ($\ell_1'/\ell_1 = 0.2$) to the mid-point of wire 1 ($\ell_1'/\ell_1 = 1.0$). To follow such poles it is necessary to calculate mode vectors in order to keep track of the same pole and assign values to the right pole. In these studies the length ℓ_2 has been maintained constant and the problems zoned such that 9 zones are always over the length ℓ_2. In Figure 4 the pole trajectories are shown as the ratio $2\ell_2/(\ell_1' + \ell_1)$ is varied from 0.444 to 1.33. The curves in Figure 5 show the motion of four poles as the radii of both wires change.

In each of the Figures 6-8 are three dimensional representations of the mode vectors for various poles. The real parts of the mode vectors lie in the z-direction while the cylinders are oriented as in Figure 2. In Figure 6 are the mode vectors for poles n = 1,2, reference case, crossed cylinders, symmetric excitation (or $\vec{E}$ parallel to y-wire). Figure 7 is similar to Figure 6 except for the n = 3 and n = 4 poles. In Figure 8 the mode vectors are plotted for four poles (whose imaginary values are designated on the figure) associated with antisymmetric excitation (or $\vec{E}$ parallel to x-wire). Due to the location of the intersection point of the wires, these modes do not couple to the y-wire and this case reduces to the isolated cylinder [3].

Figures 9 and 10 are somewhat more conventional plots of the real and imaginary parts of the first four current modes for the reference case, symmetric excitation. In the figures the y = 0 and x = 0 points have been dispaced for clarity. As discussed earlier [1,2,3,6] the charge densities can also be calculated from SEM. To do this requires knowledge of the derivatives of the current mode vectors as mentioned in the foregoing.

Figures 11 and 12 show the 3-d version of the real part of the first four charge mode vectors, Figures 13 and 14 are the complex charge mode vectors (first four) for the reference case.

From Figures 11-14 it may be noted that the induced charge per unit length is continuous through the junction region on both wires, yet the charge per unit length on the perpendicular wires is different. However, the only condition imposed on the induced charge and current is that the current on the wires at the midpoint of the junction must satisfy the Kirchhoff circuit law, i.e.

$$I_x(o+) + I_y(0+) - I_x(0-) - I_y(0-) = 0$$

other investigators have imposed in addition to the foregoing that the junction charge be uniformly distributed over the junction surface. The computations reported here do not justify that requirement, at least for the parameters that are considered.

Figures 15, 16 and 17 represent the coupling coefficients [1,2,3] for the first three poles (reference case) as a function of θ and ϕ for E-symmetric excitation.

Figure 18 is the time history of the junction current at y = 0- for one, and five poles, reference case, normal incidence. This time history and the others that are subsequently reported are those induced by a step incident pulse. The aforementioned graph indicates the rate of convergence as the number of terms included in the SEM sum increases. On the same figure is included the result of the conventional Fourier inversion technique which was previously obtained considering the frequency response from near zero up to a $k\ell_2$ value approaching 5 [7]. The comparison shown in Figure 18 must be evaluated in the manner intended. The results

obtained by SEM are derived from a formulation which includes end caps and uses sinusoidal expansion functions for the current. The Fourier results are based on the E-field Hallen integral equation formulation which does not include end caps and uses constant current expansion functions. The fact that differences occur between the results evidently is primarily due to end caps being included in one case and not in the other rather than being due to the difference between the SEM and standard Fourier techniques. As a matter of fact previously obtained results [6] show that the inclusion of end caps in this SEM problem results in the first peak being higher and somewhat more narrow with the remaining portions of the time history curves being attenuated at a slightly more rapid rate with a shift in the ringing frequency due to the electrical lengths of the wires being increased with the addition of end caps. This behavior is also seen in Figure 19 where the time histories of the junction currents at y = 0+ and x = 0+ are presented.

Figure 20 is the time history of the charge density at the end of one wire element. As discussed in previous reports [1,3,6], there are two methods by which the charge density may be calculated. In each there is a time dependent term in the form of a summation over poles. In each there is a time independent term but it is evaluated differently in the two methods. First, it can be evaluated by a limiting process ($s \to 0$) which provide the correct late time behavior; second, it can be calculated as a summation over poles. The curves in Figure 20 are the result of the latter method. The symbol D appearing on the Graph is $\varepsilon_o E_o$ the incident electric flux density. On Figure 20 the solid lines beginning at ct/L = 7.0 indicate the results of the time independent summation process as one includes one, three, and five poles in the sum. This

indicates the rate of convergence of the method to the late time behavior obtained by the limiting process which in a sense should include all pole terms. Figure 21 shows the time histories for the charge densities at the ends of the other two wire elements, $y = +\ell_1'$ and $x = \ell_2$.

Literature Cited

1. Baum, C. E., "On the Singularity Expansion Method for the Solution of Electromagnetic Interaction Problems," Interaction Note 88, Dec. 1971.
2. Baum, C. E., "On the Singularity Expansion Method for the Case of First Order Poles," Interaction Note 129, Oct. 1972.
3. Tesche, F. M., "On the Singularity Expansion Method as Applied to Electromagnetic Scattering from Thin Wires," Interaction Note 102, April 1972.
4. Martinez, J. P., Pine, Z. L., and Tesche, F. M., "Numerical Results of the Singularity Expansion Method as Applied to a Plane Wave Incident on a Perfectly Conducting Sphere," Interaction Note 112, May 1972.
5. Marin, L., "Natural Mode Representation of Transient Scattering From Rotationally Symmetric, Perfectly Conducting Bodies and Numerical Results for a Prolate Spheroid," Interaction Note 119, Aug. 1972.
6. Crow, T. T., Graves, B. D., and Taylor, C. D., "Numerical Techniques Useful in the Singularity Expansion Method as Applied to Electromagnetic Interaction Problems," Mathematics Note 27, Dec. 1972.
7. Crow, T. T. and Taylor, C. D., "Induced Electric Currents on Some Configurations of Wires; Part I, Perpendicular Crossed Wires," Interaction Note 85, Nov. 1971.
8. Shumpert, T. H., Crow, T. T., and Taylor, C. D., "Induced Electric Currents on Configurations of Thick Wires; Perpendicular Crossed Wires," Interaction Note 103, May 1972.
9. Taylor, C. D. and Wilton, D. R., "The Extended Boundary Condition Solution on the Dipole Antenna of Revolution," Interaction Note 113, June 1972.

Table 1: Natural Frequencies and Coupling Coefficients for the Reference Case

Pole Number (α)	$s_\alpha L/c$	$\eta_\alpha c/Lx10^3$
1	- .2935 + j 2.2922	9.089 + j 3.525
2	- .3356 + j 3.8392	3.768 + j 4.295
3	- .6609 + j 6.0656	1.788 + j 1.774
4	-1.0065 + j 8.1563	-3.148 - j 1.908
5	-1.1143 + j11.0767	0.637 + j 0.486

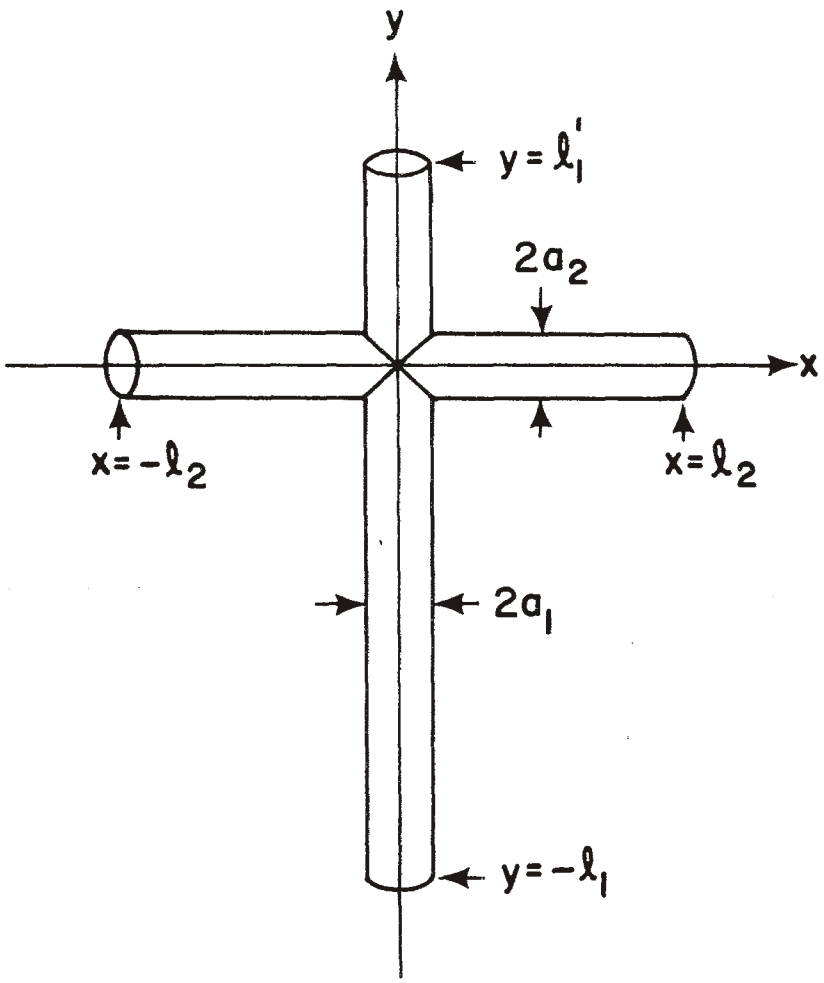

Figure 1: Crossed Thin Cylinders (Positive Current are directed in the +x and +y directions).

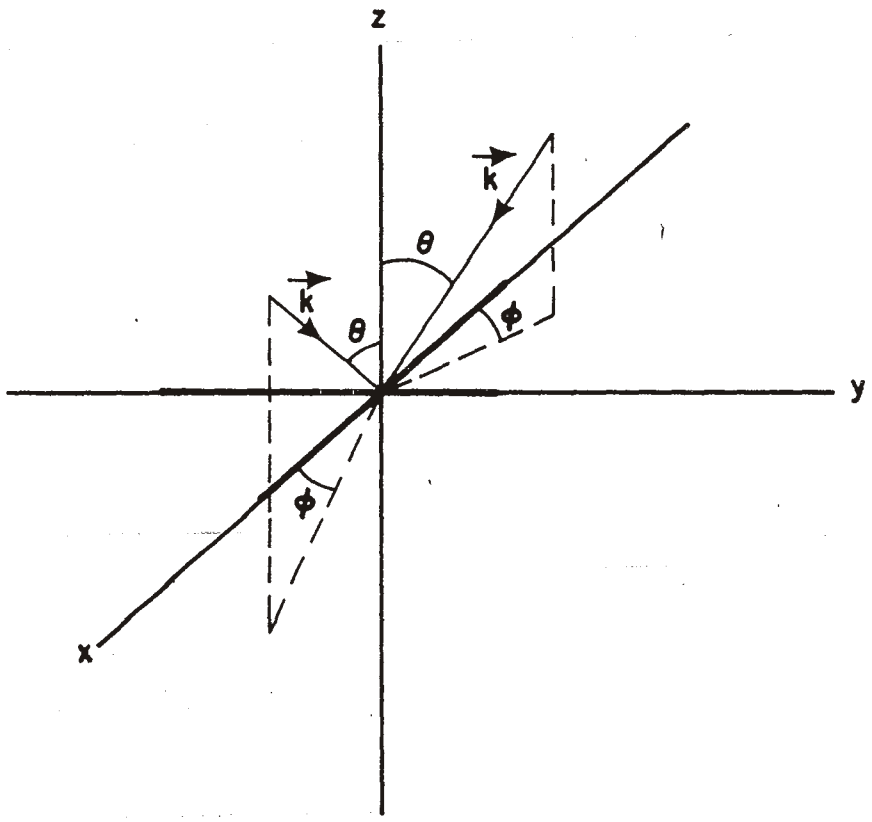

Figure 2: Crossed Thin Cylinders with Two Incident Plane Waves.

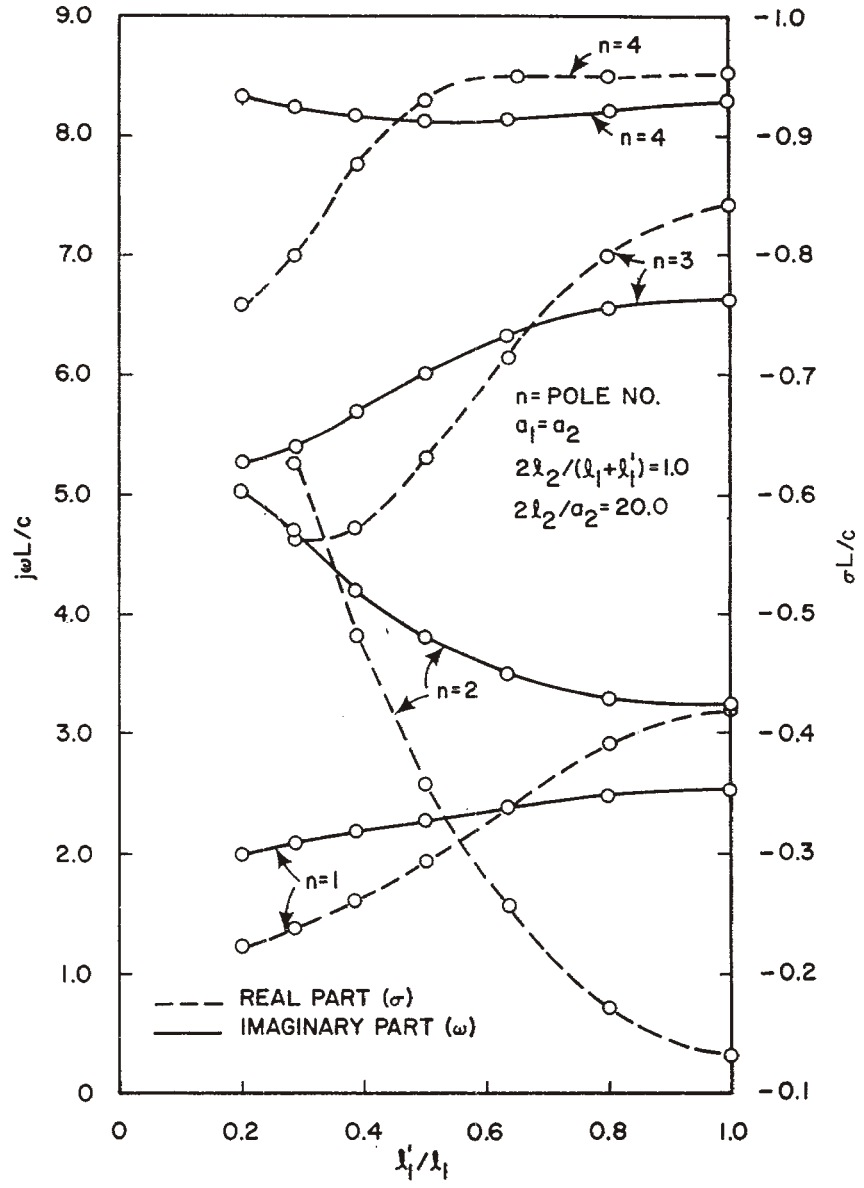

Figure 3: Pole Trajectories for Variation in the Location of the Wire Junction.

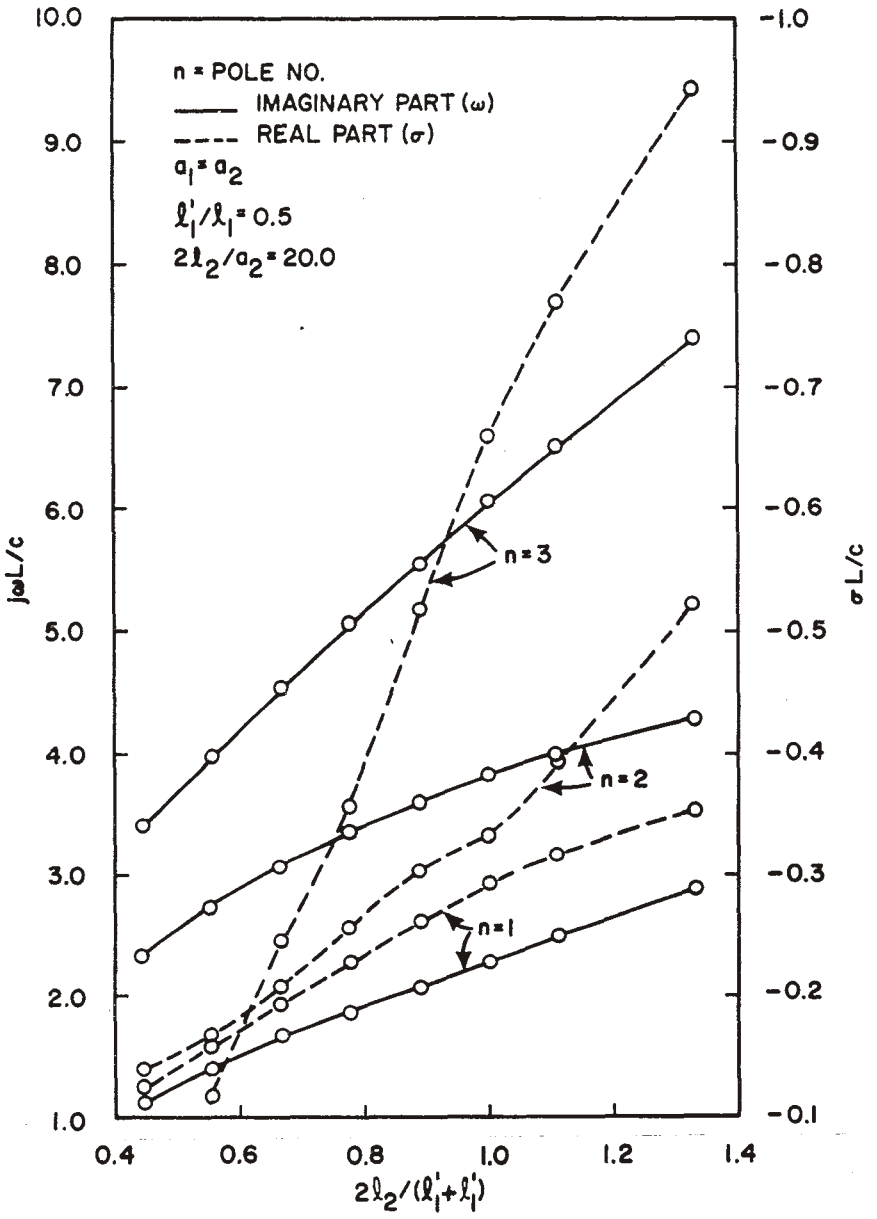

Figure 4: Pole Trajectories for Variation in the Relative Lengths of the Crossed Wires.

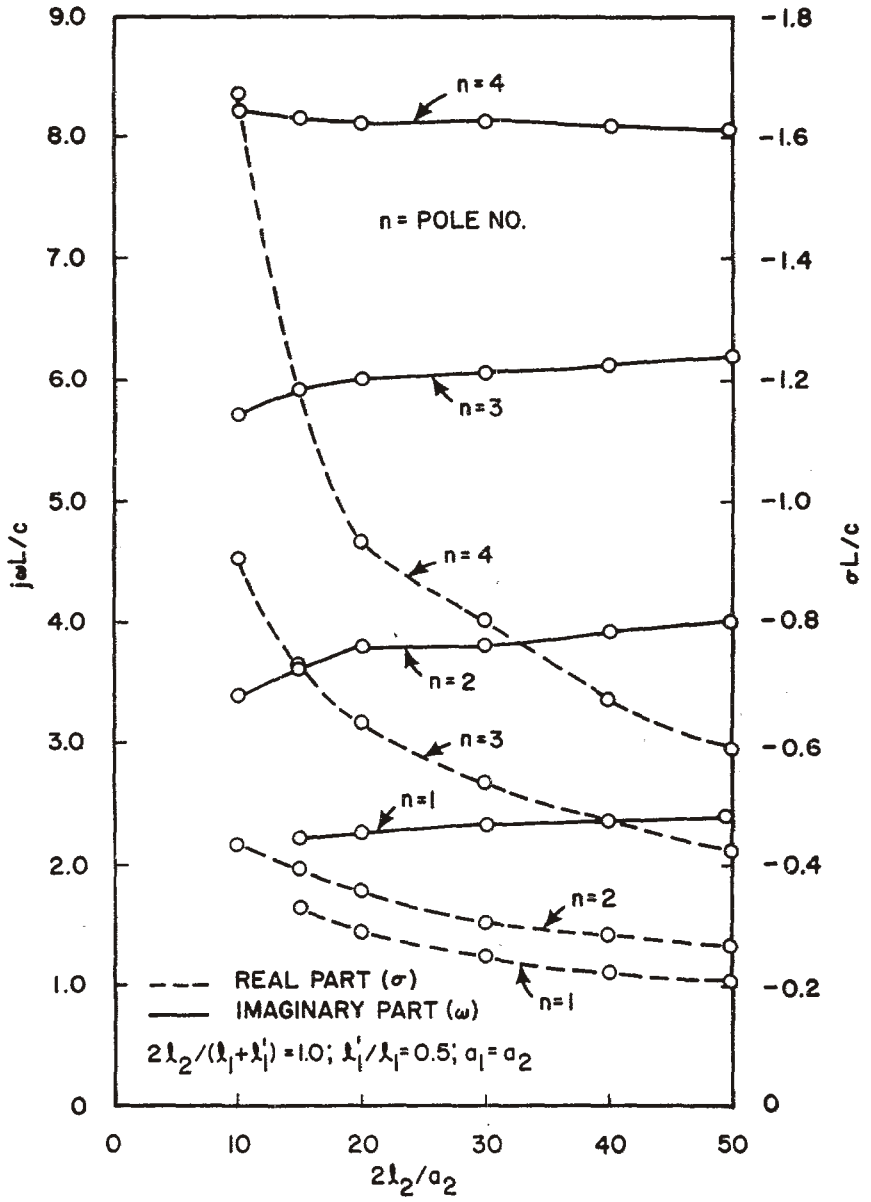

Figure 5: Pole Trajectories for Variation in the Wire Radii.

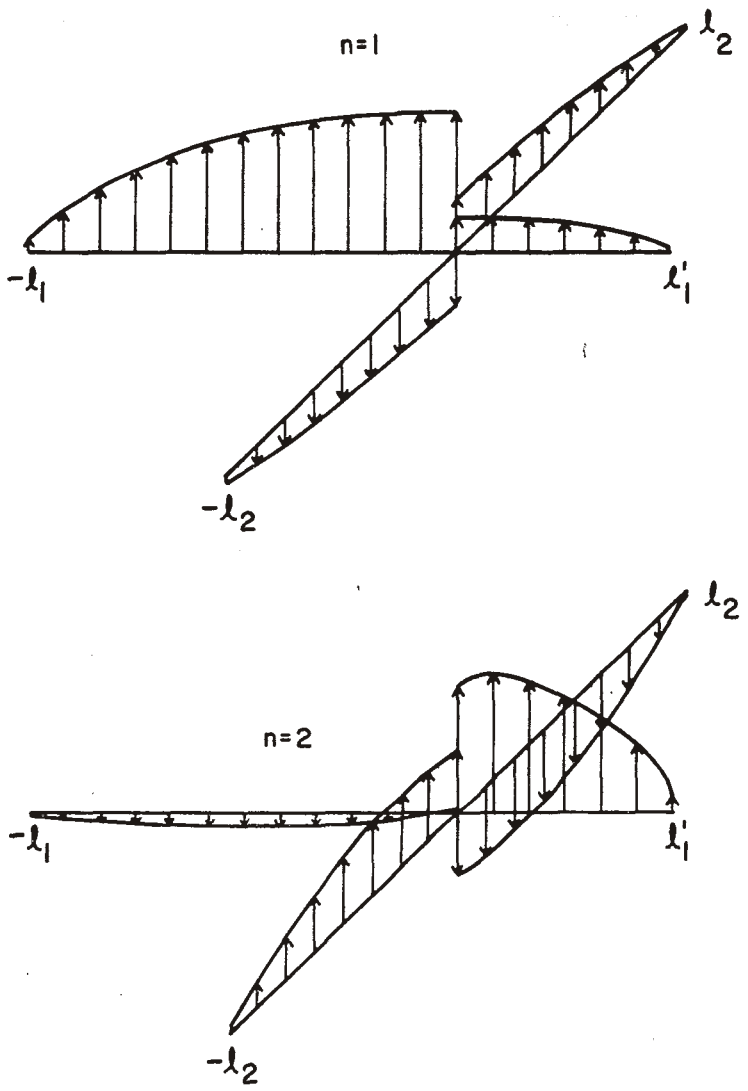

$a_1 = a_2$; $2\ell_2/(\ell_1+\ell_1') = 1.0$; $\ell_1'/\ell_1 = 0.5$; $2\ell_2/a_2 = 20.0$

Figure 6: Real Part of the Current Modes for the Reference Case.

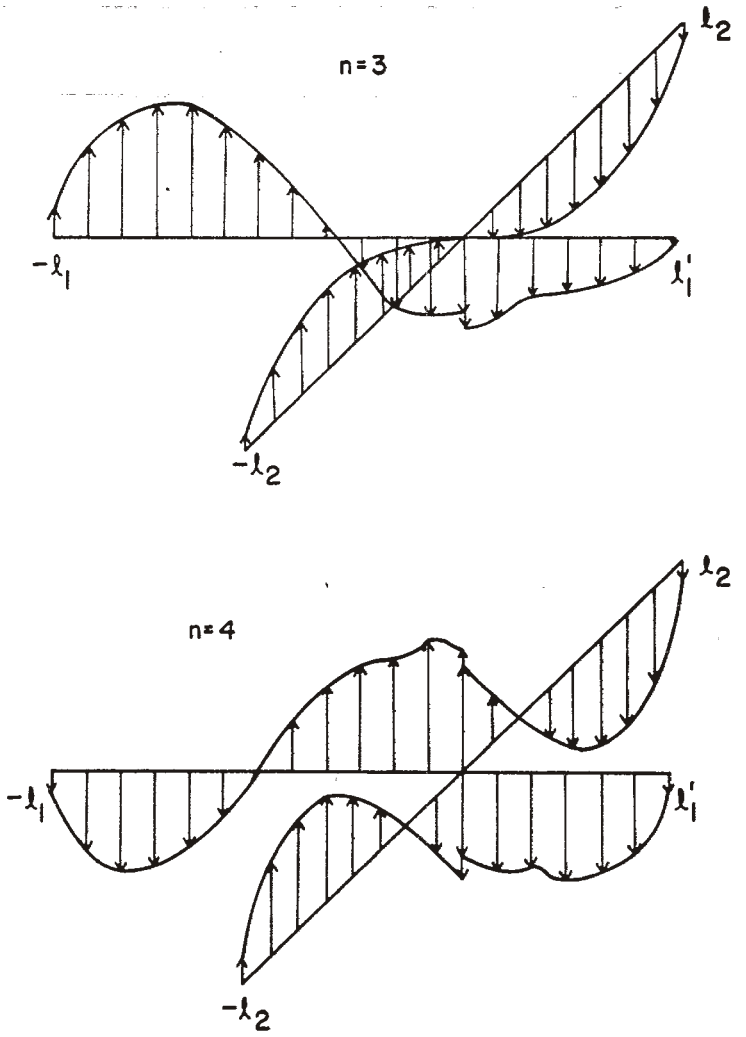

$a_1 = a_2 ; 2\ell_2/(\ell_1+\ell_1') = 1.0 ; \ell_1'/\ell_1 = 0.5 ; 2\ell_2/a_2 = 20.0$

Figure 7: Real Part of the Current Modes for the Reference Case.

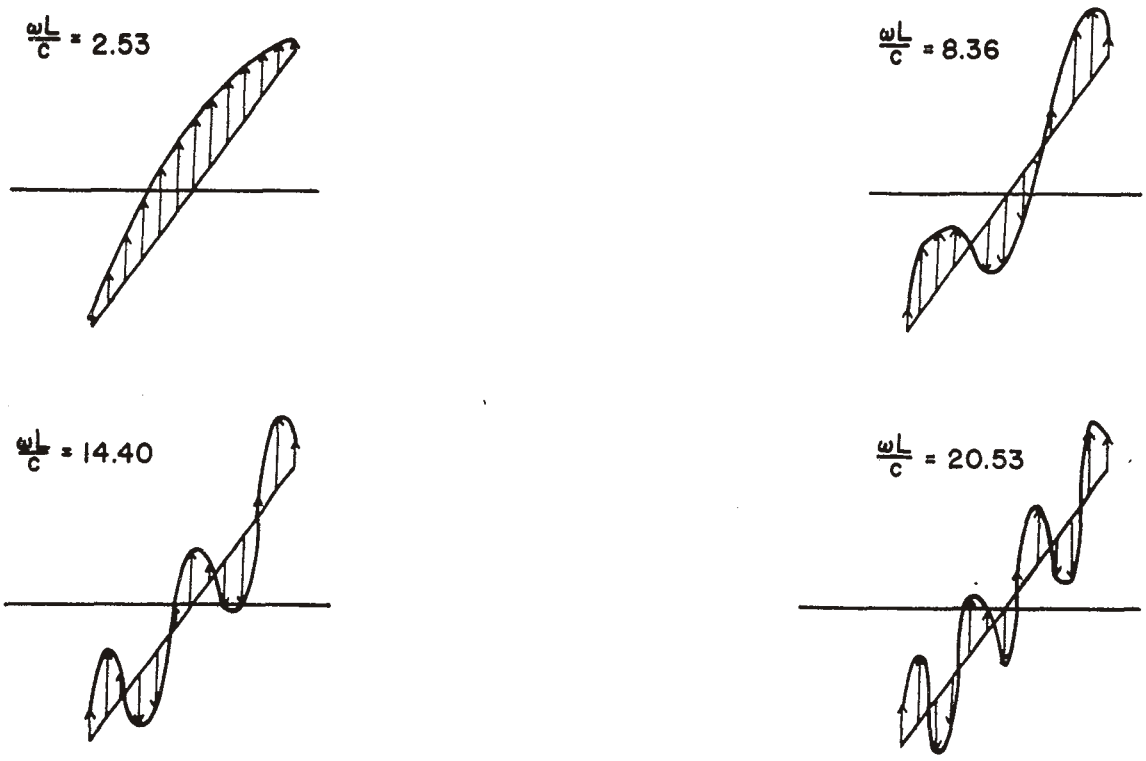

Figure 8: Real Part of the Current Modes for Antisymmetric Excitation.

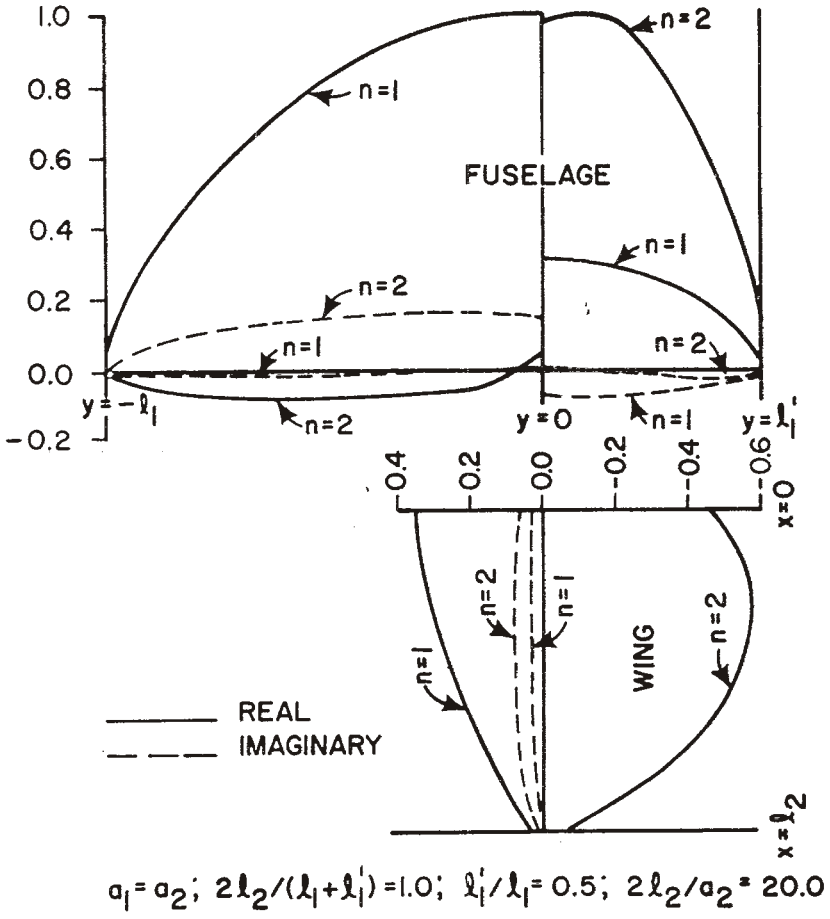

Figure 9: Current Modes for the Reference Case.

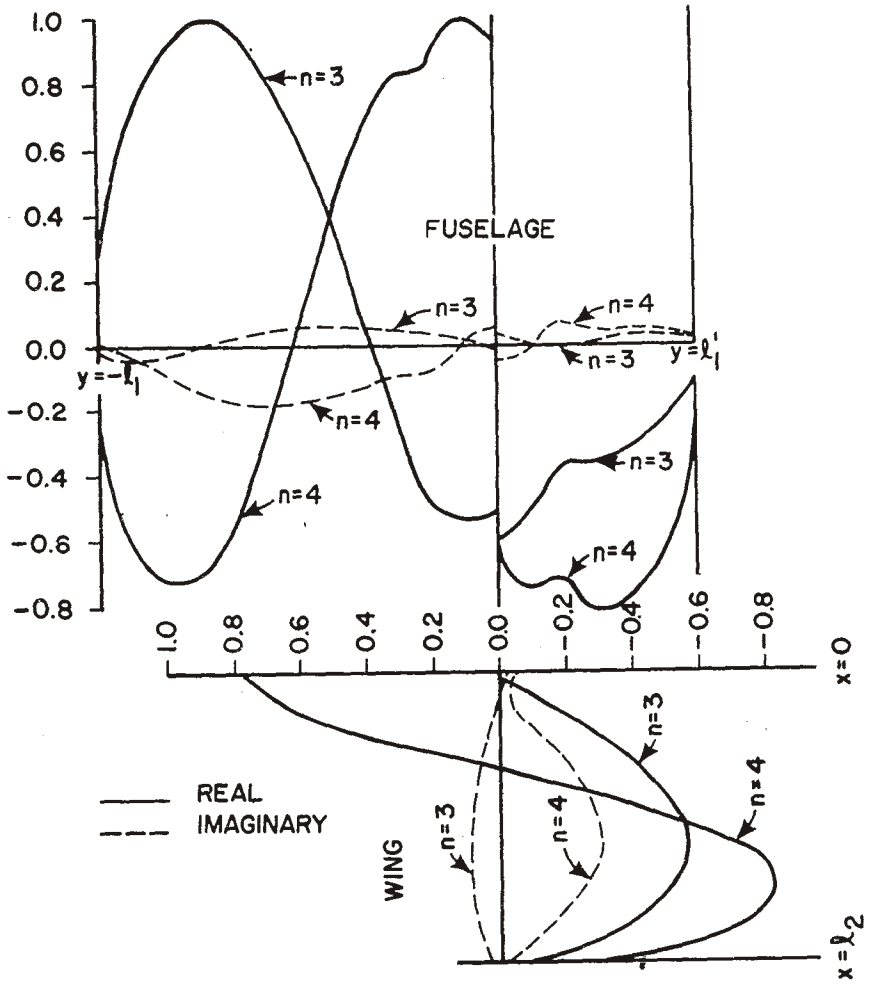

Figure 10: Current Modes for the Reference Case.

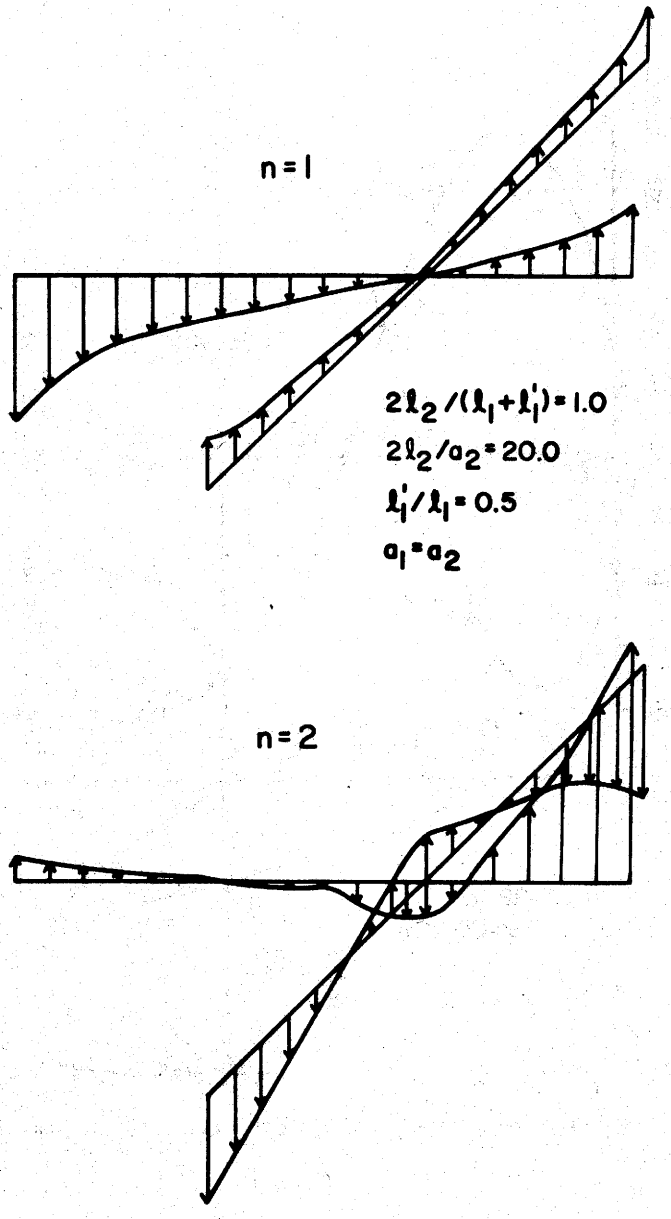

Figure 11: Real Part of the Charge Modes for the Reference Case.

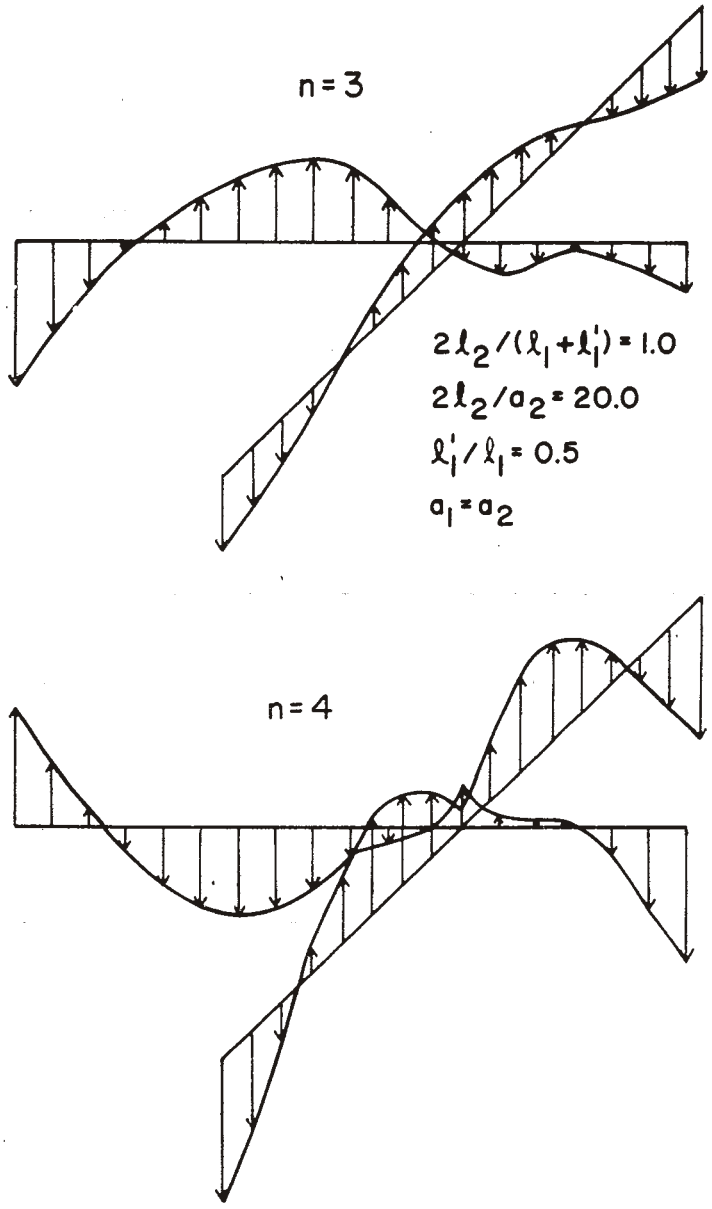

Figure 12: Real Part of the Charge Modes for the Reference Case.

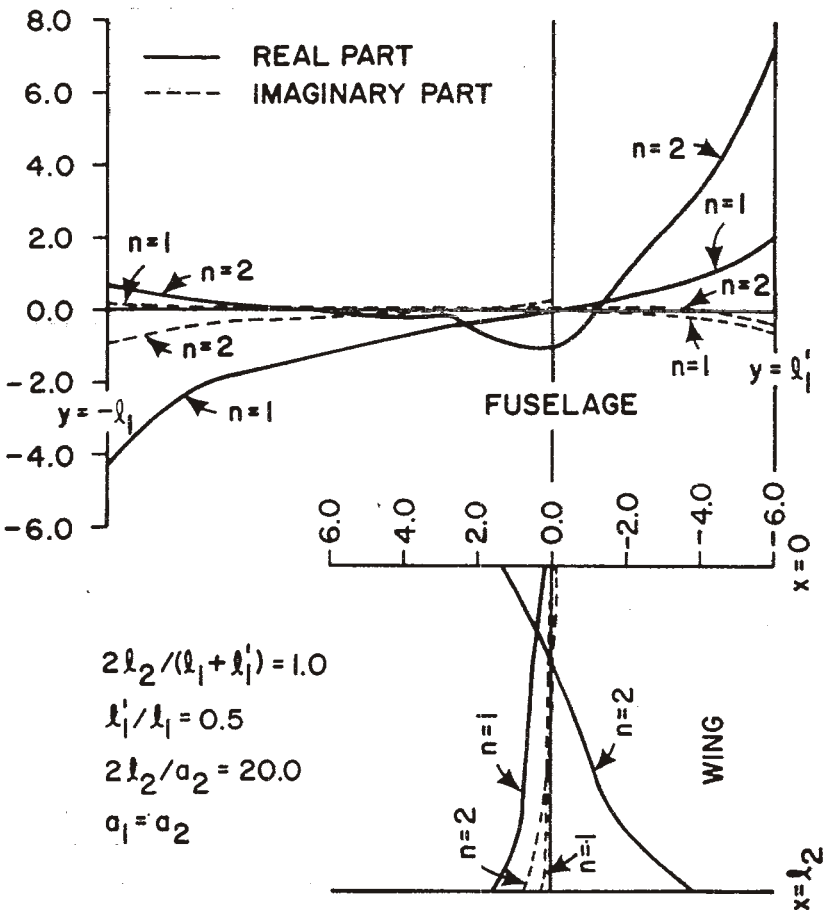

Figure 13: Charge Modes for the Reference Case.

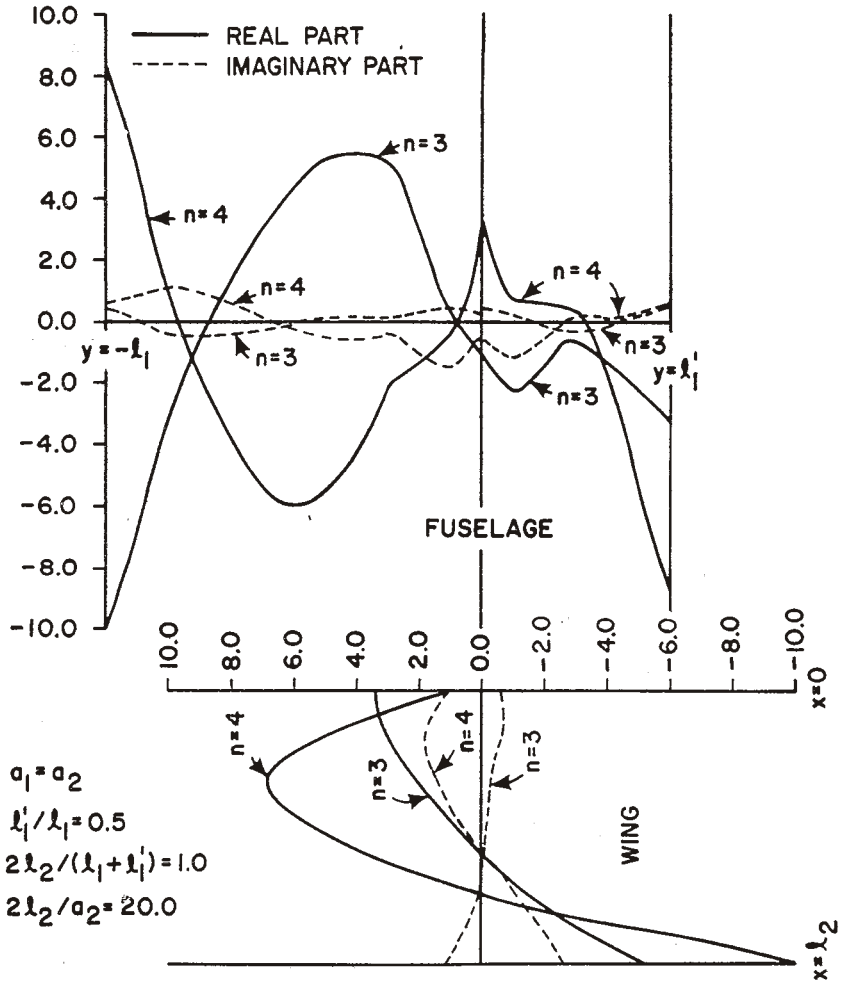

Figure 14: Charge Modes for the Reference Case.

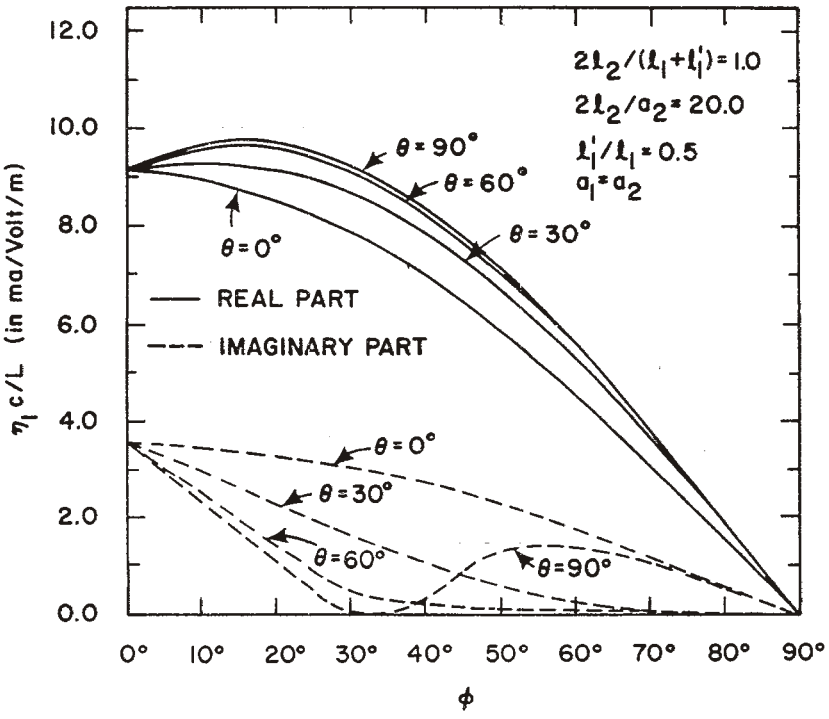

Figure 15: Complex Coupling Coefficient for the First Mode Versus Direction of Incidence.

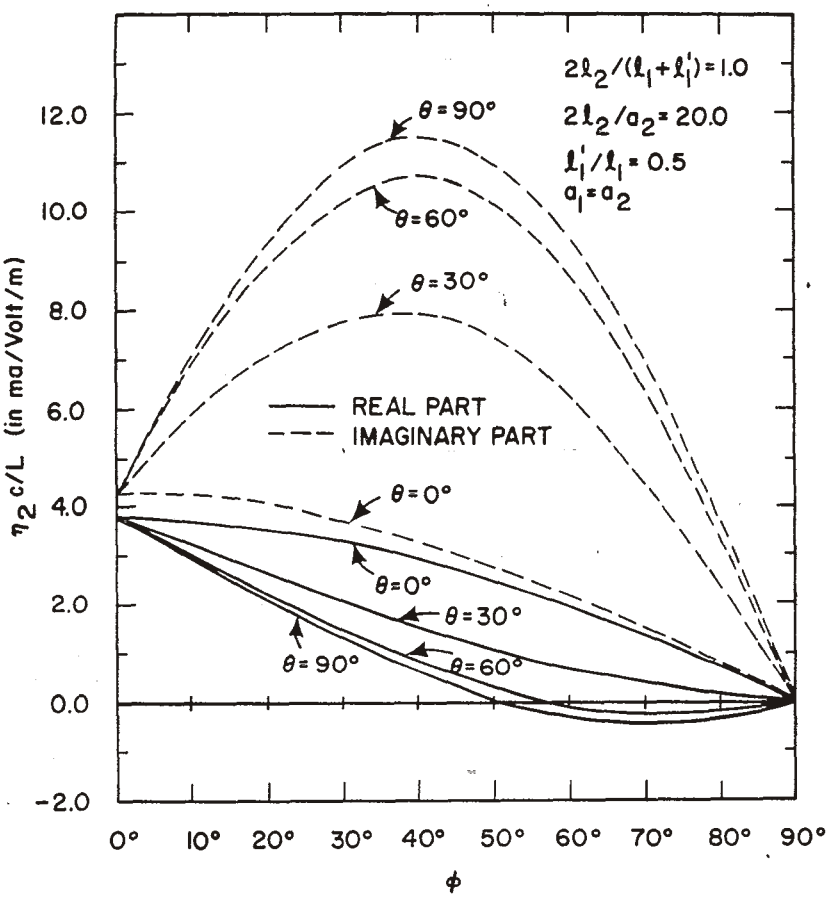

Figure 16: Complex Coupling Coefficient for the Second Mode Versus Direction of Incidence.

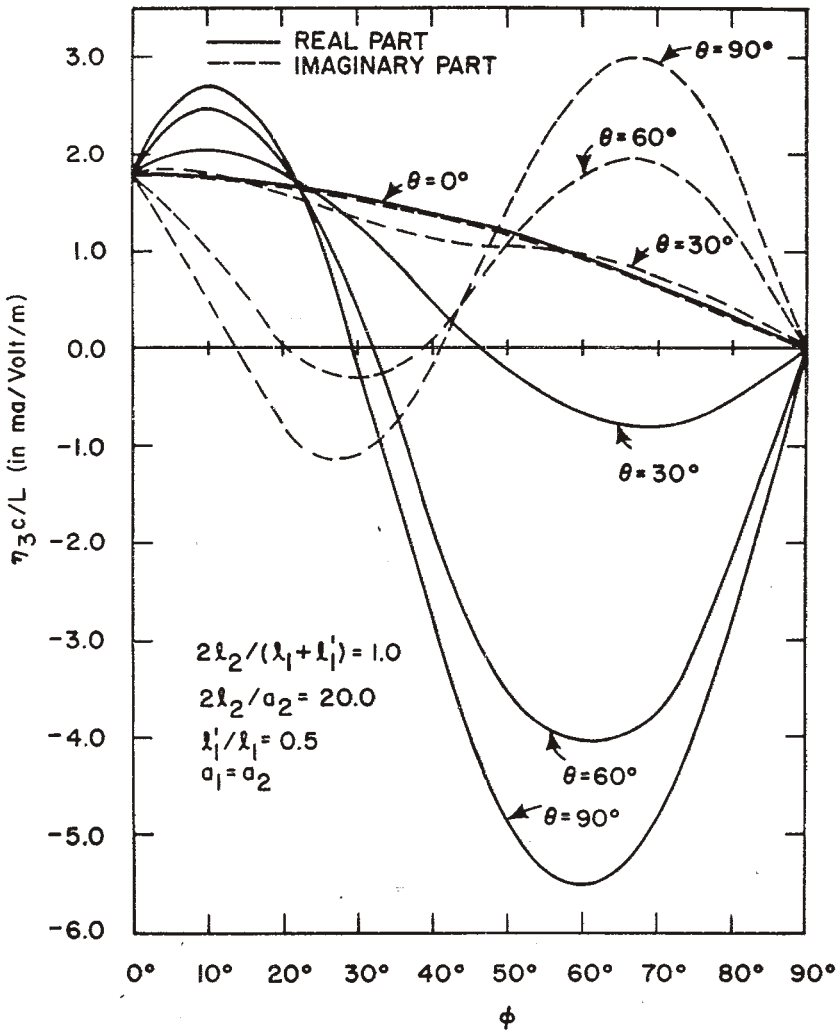

Figure 17: Complex Coupling Coefficient for the Third Mode Versus Direction of Incidence.

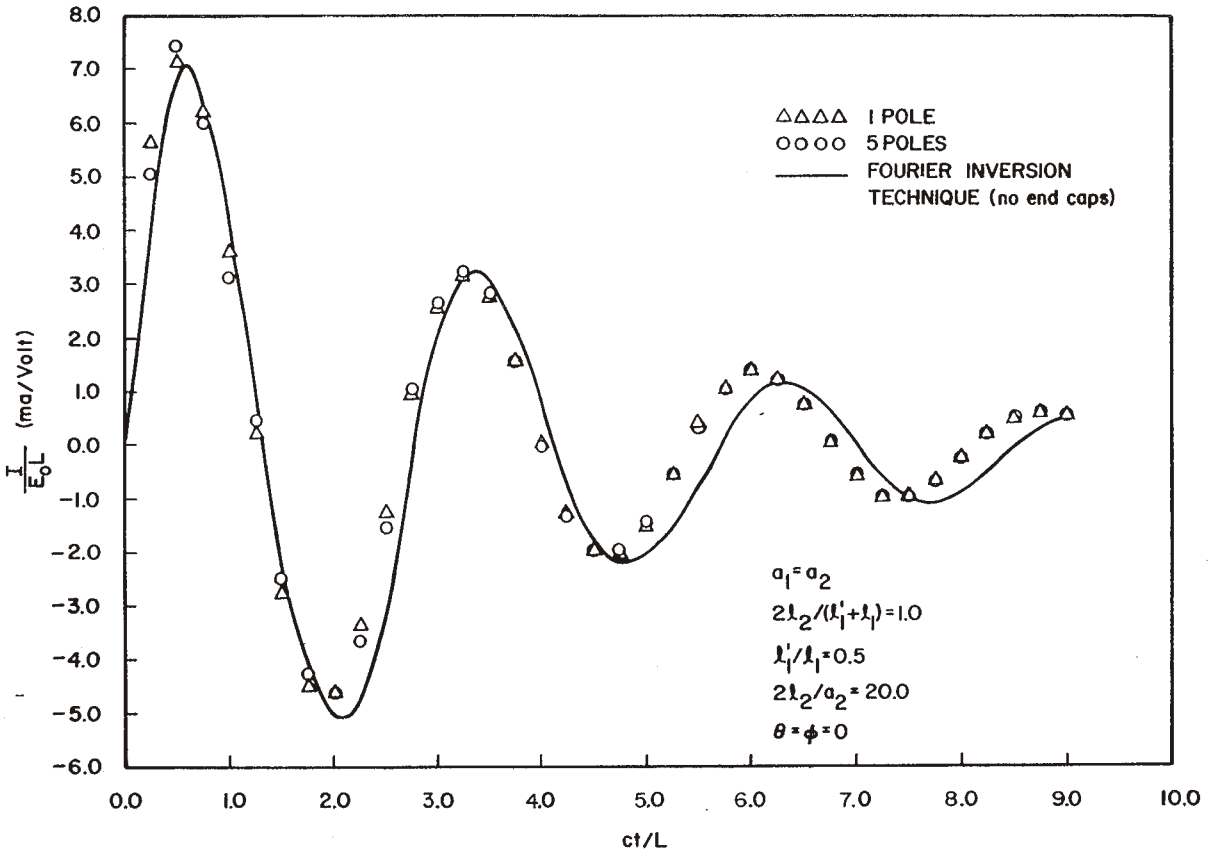

Figure 18: Time History of the Wire Junction Current at y = 0- for the Reference Case.

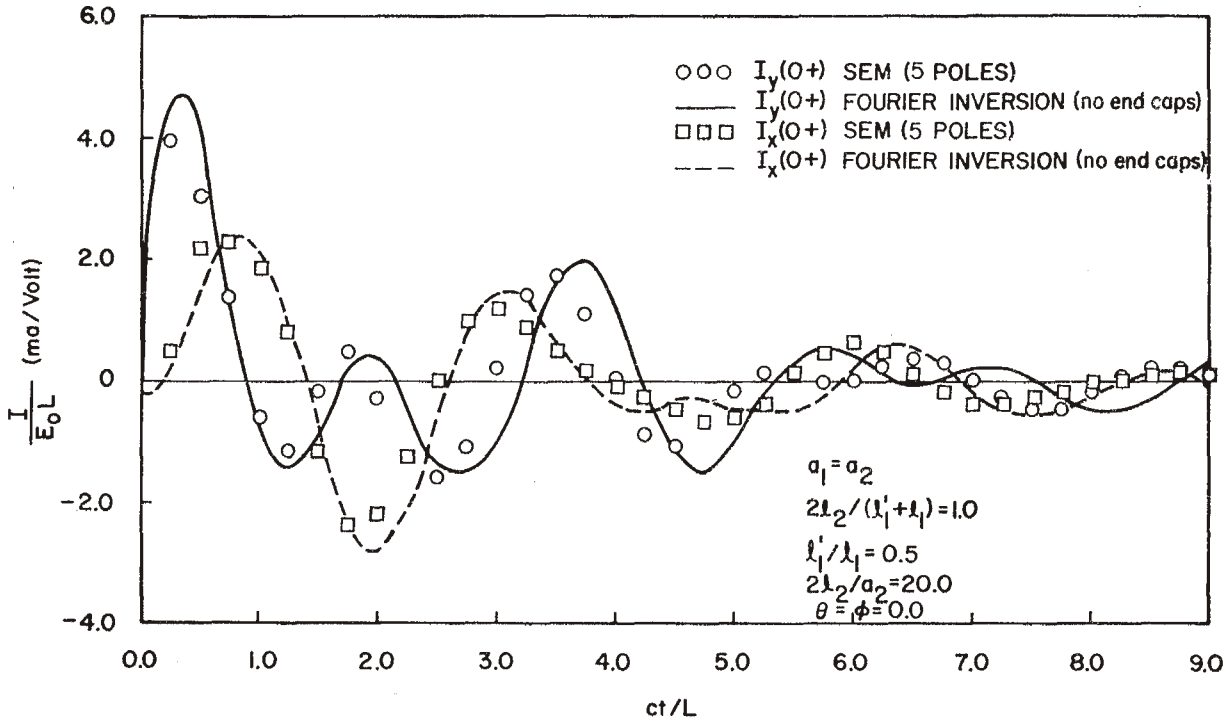

Figure 19: Time Histories of the Wire Junction Currents at y = 0+ and x = 0+ for the Reference Case.

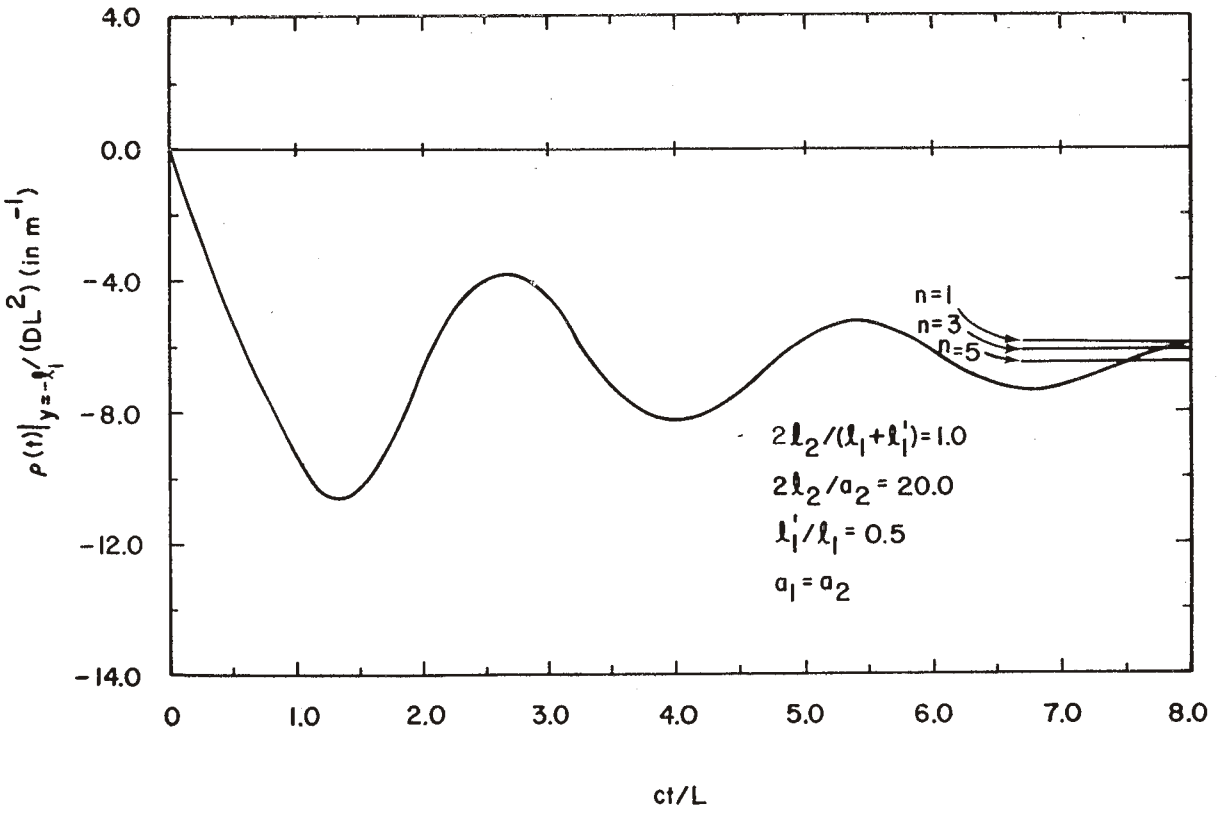

Figure 20: Time History of the Charge per Unit Length at $y = -\ell_1$ (Using 5 Poles).

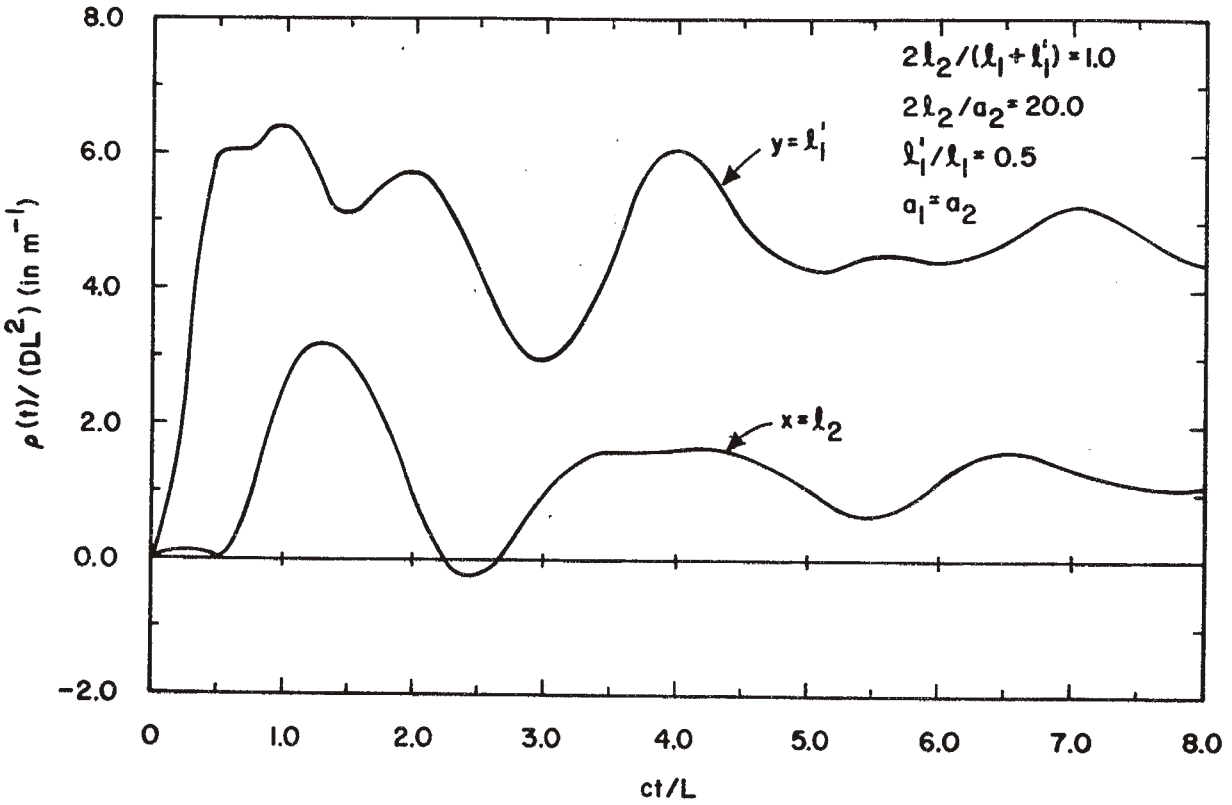

Figure 21: Time history of the Charge per Unit Length at $y = \ell_1'$ and $x = \ell_2$ (Using 5 Poles).